JOINT MODELING OF IMPEDANCE AND RADIATION AS A RECURSIVE PARALLEL FILTER STRUCTURE FOR EFFICIENT SYNTHESIS OF WIND INSTRUMENT SOUND

Esteban Maestre

CAML / CIRMMT
McGill University
Montréal, QC, Canada
`esteban@music.mcgill.ca`

Gary P. Scavone

CAML / CIRMMT
McGill University
Montréal, QC, Canada
`gary@music.mcgill.ca`

Julius O. Smith

CCRMA
Stanford University
Stanford, CA, USA
`jos@ccrma.stanford.edu`

ABSTRACT

In the context of efficient synthesis of wind instrument sound, we introduce a technique for joint modeling of input impedance and sound pressure radiation as digital filters in parallel form, with the filter coefficients derived from experimental data. In a series of laboratory measurements taken on an alto saxophone, the input impedance and sound pressure radiation responses were obtained for each fingering. In a first analysis step, we iteratively minimize the error between the frequency response of an input impedance measurement and that of a digital impedance model constructed from a parallel filter structure akin to the discretization of a modal expansion. With the modal coefficients in hand, we propose a digital model for sound pressure radiation which relies on the same parallel structure, thus suitable for coefficient estimation via frequency-domain least-squares. For modeling the transition between fingering positions, we propose a simple model based on linear interpolation of input impedance and sound pressure radiation models. For efficient sound synthesis, the common impedance-radiation model is used to construct a joint reflectance-radiation digital filter realized as a digital waveguide termination that is interfaced to a reed model based on nonlinear scattering.

1. INTRODUCTION

For robust and efficient sound synthesis, many digital waveguide models [1] of wind instruments approximate their air columns as being cylindrical. In a typical digital waveguide model, the air column of an ideal instrument constructed from a cylindrical pipe and a bell can be represented by a pair of delay lines simulating pressure wave propagation inside the pipe, and a termination that includes two digital filters: one that lumps frequency-dependent propagation losses and dispersion, and another one emulating the frequency-dependent bell reflectance. In these efficient schemes, the reed-valve end termination of the pipe is often modeled via a nonlinear scattering element that is interfaced to the air column model through decomposed pressure traveling waves P^+ and P^-, respectively going into and reflected back from the pipe input interface. Approximations with conical elements are possible [2] but often result in inharmonic resonance structures that are difficult to tune for sound synthesis [3].

To account for realistic, non-ideal instrument air column shapes, one could treat the entire air column as a resonant load, observe its linear behavior from frequency-domain experimental data, and propose a modal expansion formulation that characterizes the air column as a series association of second-order ordinary differential equations nonlinearly coupled to a partial differential equation modeling the behavior of the valve [4]. Using a state-space formulation,

the valve-resonator coupling used in such framework relies on implicit integration schemes that may cause numerical dispersion and require high computational cost. For sound synthesis purposes, our digital waveguide approach is based on coupling the valve (a nonlinear scattering element) to the resonator via pressure traveling waves. Frequency-domain measurements are used to design an *air column load* input impedance filter model $Z(z)$ (i.e., an input impedance filter) for simulation so that the pressure wave P^- reflected off the air column entrance can be obtained from the incident wave P^+ via

$$P^-(z) = R(z)P^+(z), \tag{1}$$

where $R(z)$ is a digital reflectance model derived from $Z(z)$. The input impedance frequency response

$$Z(\omega) = \frac{P(\omega)}{U(\omega)}, \tag{2}$$

where $P(\omega)$ and $U(\omega)$ respectively correspond to the frequency response of the sound pressure and flow, both at the entrance of the air column. In a previous work [5], a frequency-domain measurement of an air column input impedance is used to construct a discrete-time reflection function $r[n]$ that is suitable for a traveling-wave numerical scheme based on convolution. In that paper, the authors propose a workaround method to evade time-aliasing and other numerical problems that naturally arise from estimating $r[n]$ via inverse Fourier transform of a frequency-domain measurement signal.

This work avoids the aforementioned problems by proposing a methodology for translating an input impedance measurement directly into a recursive digital filter $Z(z)$ of moderately low order, with the added advantage that efficiency is improved with respect to discrete convolution. Moreover, we are interested in using external sound pressure measurements to design a sound pressure radiation filter $E(z)$ able to model how the flow at the entrance of the air column is related to the sound pressure radiated to an external position in the vicinity of the instrument. This paper is an extension of a recent preliminary work [6] were we used the saxophone impedance measurement of a sole fingering position to propose a methodology for designing an impedance parallel filter, and its realization as a reflectance. Here, after taking a full set of measurements including input impedance and sound pressure radiation for all fingering positions, we propose a radiation model in parallel form and revise the reflectance filter formulation to include radiation, leading to a joint reflectance-radiation digital filter formulation with similar properties to those of a recently introduced admittance-radiation model for string instruments [7]. Moreover, we propose a simple model for fingering transitions that is based on linear interpolation of impedance and radiation digital filters. For completeness, this

paper revisits the methodology for designing the impedance filter already introduced in [6].

In a hemi-anechoic space, alto saxophone input impedances were measured using a six-microphone probe calibrated with three non-resonant loads via a least-mean square signal processing technique as described in [8]. Simultaneously, an external measurement microphone was placed near the bell of the instrument to record the radiated sound pressure signal. A sound pressure radiation frequency response $E(\omega)$ was defined in the frequency-domain as

$$E(\omega) = \frac{T(\omega)}{U(\omega)}, \qquad (3)$$

where frequency-domain functions $T(\omega)$ and $U(\omega)$ respectively correspond to the radiated sound pressure signal at a point in the external radiation domain (i.e., the signal recorded with the microphone) and the signal of the flow at the entrance of the air column. With this in mind, we aim at constructing a radiation modeling filter $E(z)$ such that the (external) radiated sound pressure $T(z)$ can be obtained from the simulated scalar flow $U(z)$ as $T(z) = E(z)U(z)$.

In Figure 1 we display the magnitude response of some of the measurements, in particular for fingerings E-5 (natural E5), Bb4 (B4-flat), and C#6 (C6-sharp). In the top plots appear the impedance transfer functions, normalized to the characteristic wave impedance of the air column input. As the resonance amplitudes decrease with frequency, the normalized impedance tends to a value of 0 dB, i.e., total transmission. In the bottom plots appear the corresponding radiation transfer functions, where it is possible to observe a shared modal structure with the impedance. This observation motivates the pursuit of a joint formulation for impedance and radiation modeling, and that constitutes the main focus of this work.

The outline is as follows. In Sections 2 and 3 we re-introduce our input impedance model and its optimization-based design technique as it was first described in [6], with slight nomenclature changes that will help in following the rest of the paper. Then, we follow in Section 4 by introducing the sound pressure radiation model. Section 5 provides details on how to jointly realize the input impedance and external radiation models as a common parallel filter in the form of a digital waveguide reflectance. In 6 we present a simple model for emulating the transition between two fingering positions. In Section 7 we briefly describe how to couple the filter to a valve model for efficiently obtaining sound. We conclude in Section 8 by pointing to future experiments and extensions.

2. INPUT IMPEDANCE MODELING

From observation of the resonance structure exhibited by the input impedance and sound radiation measurements, we propose a digital filter formulation akin to the discretization of a modal expansion. Thus, instead of relying on a digital waveguide representation of the air column, we use a different modal structure for each of the F fingering positions analyzed. For each f-th fingering case, we construct an input impedance parallel model $Z|_f(z)$ by creating a basis of $M|_f$ parallel sections each corresponding to a mode, and use the basis over which to project impedance measurements. In the f-th input impedance model, each m-th modal basis parallel section $H|_{f,m}(z)$ is defined as

$$H|_{f,m}(z) = \frac{1 - z^{-1}}{(1 - p|_{f,m}z^{-1})(1 - \bar{p}|_{f,m}z^{-1})}, \qquad (4)$$

which corresponds to a one-zero, two-pole resonator with the zero locked at DC. The resonator is defined by a pair of complex conjugate poles $p|_{f,m}$ and $\bar{p}|_{f,m}$, which we relate to the corresponding modal frequency $\nu|_{f,m}$ and bandwidth $\beta|_{f,m}$ (both expressed in Hz) by $2\pi\nu|_{f,m}T_s = \angle p|_{f,m}$ and $\beta|_{f,m} = -\log(|p|_{f,m}|)/\pi$, with T_s being the sampling period. The impedance model $Z|_{f,m}(z)$ is then formulated in parallel as

$$Z|_f(z) = \sum_{m=1}^{M|_f} (b_0|_{f,m} + b_1|_{f,m}z^{-1})H|_{f,m}(z), \qquad (5)$$

where $b_0|_{f,m}$ and $b_1|_{f,m}$ are real-valued coefficients that allow control of both the amplitude and the phase of the the m-th resonator. The main reason behind the choice for our parallel resonator structure is that, while enabling the control of the relative phase between resonators, it imposes a gain of zero at DC irrespective of the coefficients $b_0|_{f,m}$ and $b_1|_{f,m}$. Next we introduce an optimization technique to find the pole positions and numerator coefficients of model (5) given an impedance measurement. For simplicity, in Section 3 we omit the use of the sub-index f for indicating the fingering case, as the methodology presented therein applies to all F fingering cases.

3. INPUT IMPEDANCE FILTER DESIGN

Departing from a target input impedance measurement $\hat{Z}$, the problem of designing the coefficients of the impedance filter model of M digital resonators which approximates the measurement can be stated as the minimization of an error measurement $\varepsilon(Z, \hat{Z})$ between the measurement and the model, with parameters being a vector

$$\boldsymbol{p} = \{p|_1, \cdots, p|_m, \cdots, p|_M\} \qquad (6)$$

of complex poles each corresponding to the m-th resonator of the model, and vectors

$$\mathbf{b}_0 = \{b_0|_1, \cdots, b_0|_m, \cdots, b_0|_M\} \qquad (7)$$

$$\mathbf{b}_1 = \{b_1|_1, \cdots, b_1|_m, \cdots, b_1|_M\} \qquad (8)$$

of respective numerator coefficients. We solve this problem via sequential quadratic programming [9]. At each iteration only pole positions are exposed as the variables to optimize: once they are decided, zeros (i.e., numerator coefficients) are constrained to minimize an auxiliary quadratic cost function, resulting in a simple closed-form solution. The positions of the poles are optimized iteratively: at each step, an error function is successively evaluated by projecting the target frequency response over a basis of frequency responses defined by the pole positions under test. We add a set of linear constraints to guarantee feasibility and to ease convergence. This routine is extended from the filter design technique of [10] as used in [7] to model string instrument input admittances.

3.1. Impedance measurement pre-processing

As it can be observed in the grey curves of Figure 2, the high-frequency region of an impedance measurement typically presents artifacts caused by noise and limitations of the measurement method. It is important to remove those artifacts so that the target normalized impedance effectively tends to 1 as frequency increases. This is needed to help the fitting process in providing an impedance model design for which the normalized impedance also tends to 1 in the
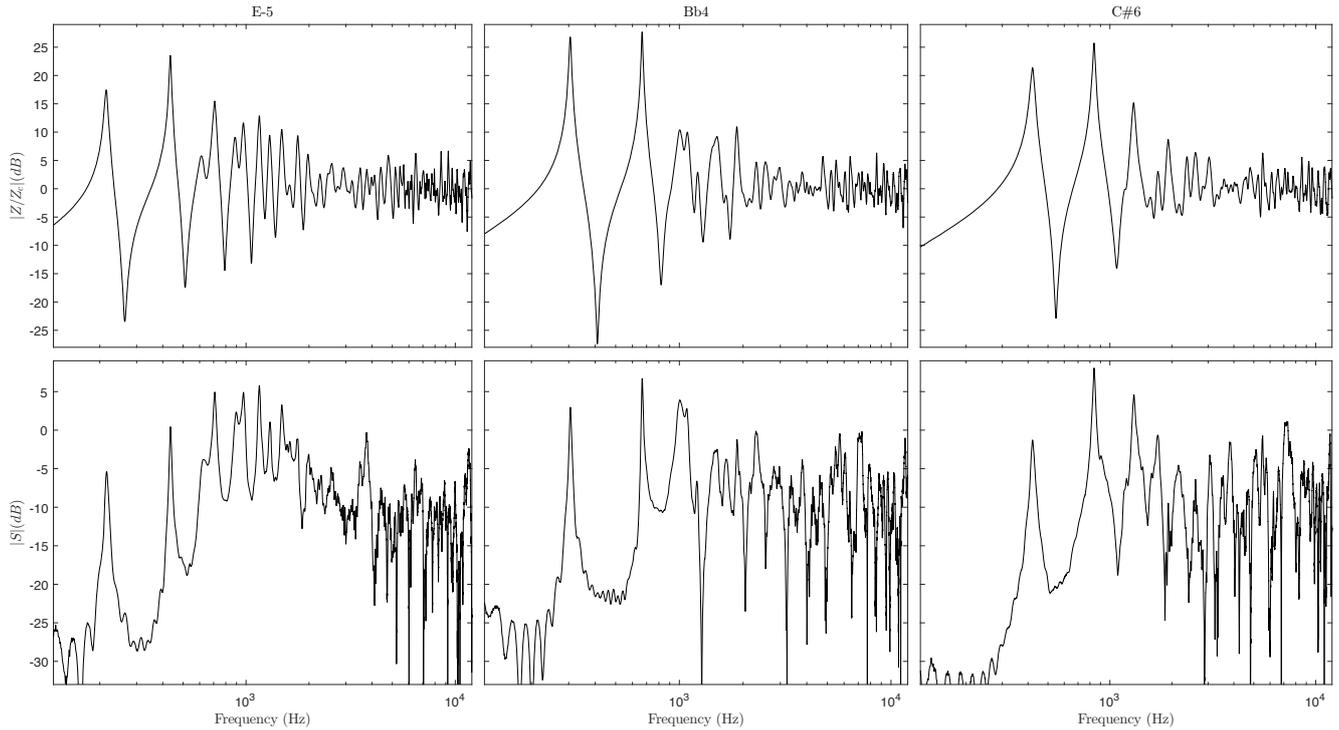
Figure 1: *Magnitude response of impedance (top) and radiation (bottom) measurements for different fingering positions in an alto saxophone.*

high frequency region; otherwise, a derived air column reflectance filter would deliver reflected pressure waves with significant energy around Nyquist, and therefore cause undesired behaviors in the reed-valve nonlinear scattering model. To this end, we perform cross-fading between the normalized impedance measurement and a constant value of one, as illustrated in Figure 2.

3.2. Optimization problem setup

We initialize the model parameters via finding a set of initial pole positions by attending to the magnitude response of the impedance measurement. First, resonance peak selection in the low-frequency region is carried out through an automatic procedure that iteratively rates and sorts spectral peaks by attending to a salience descriptor. For estimating modal frequencies, three magnitude samples (respectively corresponding to the maximum and its adjacent samples) are used to perform parabolic interpolation around selected peaks. For estimating bandwidths, the *half-power* rule [1] is applied using a linear approximation. For the high-frequency region we spread an additional set of poles, uniformly distributed on a logarithmic frequency axis. This leads to a total M modes, each parameterized by a complex pole pair in terms of its angle parameter $w|_m = |\angle p|_m|$ and its radius parameter $s|_m = -\log(1 - |p|_m|)$. This leads to two parameter sets: a set $\boldsymbol{w} = \{w|_1 \cdots w|_m \cdots w|_M\}$ of angle parameter values, and a set $\mathbf{s} = \{s|_1 \cdots s|_m \cdots s|_M\}$ of radius parameter values. With the new parametrization, we state the problem as

$$\underset{\boldsymbol{w},\mathbf{s}}{\text{minimize}} \quad \varepsilon(Z, \hat{Z}) \qquad (9)$$
$$\text{subject to} \quad \mathbf{C},$$

where $\mathbf{C}$ is a set of linear constraints, and numerator coefficients have been left out as they are not exposed as variables in the optimization. A key step before constraint definition is to sort the pole parameter sets so that linear constraints can be defined in a straightforward manner to ensure that the arrangement of poles in the unit disk is preserved during optimization, therefore reducing the number of crossings over local minima. Elements in sets $\mathbf{w}$ and $\mathbf{s}$ are jointly sorted as pairs (each pair corresponding to a complex-conjugate pole) by ascending angle parameter $w|_m$.

From ordered sets $\boldsymbol{w}$ and $\mathbf{s}$, linear constraints $\mathbf{C}$ are defined as follows. First, feasibility is ensured by $0 \leq s|_m$ and $0 \leq w|_m \leq \pi$. Second, to aid convergence we constrain the pole sequence order in set $\boldsymbol{w}$ to be respected. This is expressed by $w|_{m-1} < w|_m < w|_{m+1}$. Moreover, assuming that initialization provides an already trusted first solution, we can bound the search to a region around the initial pole positions. This can be expressed via the additional inequalities $w|_m^- < w|_m < w|_m^+$ and $s|_m^- < s|_m < s|_m^+$, where '−' and '+' superscripts are used to respectively indicate lower and upper bounds.

3.3. Error estimation

At each i-th step of the optimization, the error $\varepsilon(Z, \hat{Z})$ is estimated as follows. Given K samples of the target impedance frequency response $\hat{Z}(\omega)$ and the set $\mathbf{p}$ of M complex poles defining the modes at the i-th step, numerator coefficient vectors $\mathbf{b}_0$ and $\mathbf{b}_1$ can be obtained via least-squares by

$$\underset{\mathbf{b}}{\text{minimize}} \|\mathbf{Hb} - \hat{\mathbf{z}}\|^2, \qquad (10)$$
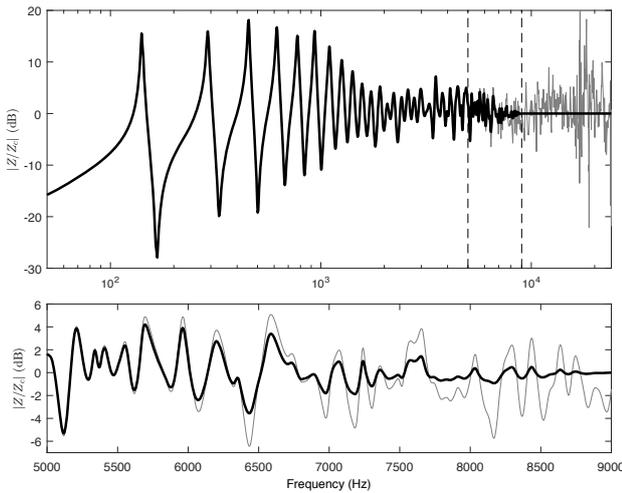
Figure 2: *Magnitude response of an alto saxophone impedance measurement (Bb3 fingering), normalized by the characteristic impedance of the input of the air column. Thin and thick curves are respectively used for raw and pre-processed data. Top: full band, with cross-fading region delimited by vertical lines. Bottom: cross-fading region.*

where $\mathbf{b} = [\,\mathbf{b}_0^T\,\mathbf{b}_1^T\,]^T$ is a real-valued vector; $\hat{\mathbf{z}}$ contains K frequency-domain samples of the impedance measurement $Z(\omega)$ at frequencies $0 \leq \omega_k < \pi$, i.e., $\hat{z}_k = \hat{Z}(\omega_k)$; and $\mathbf{H}$ is a $K \times 2M$ matrix of basis vectors constructed as

$$\mathbf{H} = [\,\mathbf{h}_0|_1 \cdots \mathbf{h}_0|_m \cdots \mathbf{h}_0|_M \, \mathbf{h}_1|_1 \cdots \mathbf{h}_1|_m \cdots \mathbf{h}_1|_M\,] \quad (11)$$

with column vectors $\mathbf{h}_0|_m$ and $\mathbf{h}_1|_m$ containing the sampled frequency responses of $H|_m(z)$ and $z^{-1}H|_m(z)$ respectively. With numerator coefficients, we evaluate the frequency response of the model and compute the error measure as the l_2-norm of the difference vector, i.e., $\varepsilon(Z, \hat{Z}) = \|\mathbf{H}\mathbf{b} - \hat{\mathbf{z}}\|^2$.

3.4. Final solution

Once poles have been optimized, numerator coefficients of model (5) are found by solving again problem (10). In Figure 3 we display the magnitude and phase responses (top and middle plots) of three example impedance models, respectively obtained from normalized impedance measurements after pre-processing. Although in principle the model (5) is not guaranteed to be positive-real, fitting to measurements of positive-real functions generally provides positive-real designs, as it can be observed from the phase responses. This is important for the stability of the sound synthesis model, as the impedance is going to be realized as a reflectance filter.

4. SOUND PRESSURE RADIATION FILTER

Given the shared modal structure observed in the input impedance and radiation measurements of each fingering, we opt for a radiation model that shares the parallel resonator structure of the impedance model $Z|_f(z)$. We define the sound pressure radiation filter $E|_f(z)$

of the f-th fingering position as

$$E|_f(z) = \sum_{m=1}^{M|_f} (d_0|_{f,m} + d_1|_{f,m}z^{-1})H|_{f,m}(z), \quad (12)$$

where the $M|_f$ modal basis parallel sections $H|_{f,m}(z)$ are shared with the impedance model (see (4) and (5)), and $d_0|_{f,m}$ and $d_1|_{f,m}$ are real-valued coefficients.

Once the pole positions that define all $H|_{f,m}(z)$ resonators have been found through optimization of the input impedance model $Z|_f(z)$ (see Section 3), numerator coefficients of $E|_f(z)$ are estimated by least-squares. First, in a pre-processing step, all radiation transfer functions are converted to minimum-phase using the real cepstrum [1]. Then, in an analogous manner as for the numerator coefficients of the input impedance model, $d_0|_{f,m}$ and $d_1|_{f,m}$ are arranged into vectors $\mathbf{d}_0|_f$ and $\mathbf{d}_1|_f$ as in (7), (8) and found by solving

$$\underset{\mathbf{d}|_f}{\text{minimize}}\|\mathbf{H}|_f\mathbf{d}|_f - \hat{\mathbf{e}}|_f\|^2, \quad (13)$$

where $\mathbf{d}|_f = [\,\mathbf{d}_0|_f^T\,\mathbf{d}_1|_f^T\,]^T$ is a real-valued column vector; $\hat{\mathbf{e}}|_f$ contains K frequency-domain samples of the radiation measurement $E|_f(\omega)$ at frequencies $0 \leq \omega_k < \pi$, i.e., $\hat{e}_k|_f = \hat{E}|_f(\omega_k)$; and $\mathbf{H}|_f$ is the $K \times 2M$ matrix of basis vectors in (11) that was used for solving the impedance projection problem (13) corresponding to the f-th fingering case. In Figure 3 we display the magnitude responses (bottom plots) of three example radiation models, along with their corresponding impedance models, overlaid on the measurements. A similar quality of approximation was also observed in all other fingering positions.

5. JOINT REALIZATION AS A WAVEGUIDE TERMINATION

From the input impedance model (5), we construct a reflectance that keeps the state of the air column as a resonating element, and allows us to obtain reflected waves from its interface. The formulation that we propose involves the computation of the flow as an intermediate step, therefore allowing us to obtain the external radiated sound pressure as $T(z) = E(z)U(z)$ via model (12). Since both the impedance model and the sound pressure radiation model are constructed so that they share the exact same set of parallel resonators, obtaining the radiated sound comes at a very low additional cost. Thus, via a single set of $M|_f$ resonators corresponding to the f-th fingering position, we are able to model pressure wave reflectance, radiated sound pressure, and (implicitly) energy loss from input transmittance to non-radiating modes and dissipation.

5.1. Reflectance realization

Following the digital waveguide formulation for loaded parallel junctions [1], we can compute the scalar flow $U(z)$ at the input of the air column solely from the input pressure wave $P^+(z)$ as

$$U(z) = \frac{2Y_c P^+(z)}{1 + Y_c Z|_f(z)} \quad (14)$$

where Y_c is the characteristic admittance of the input of the air column, and $Z|_f(z)$ is the input impedance model corresponding to the f-th fingering position. From the flow $U(z)$, it should be
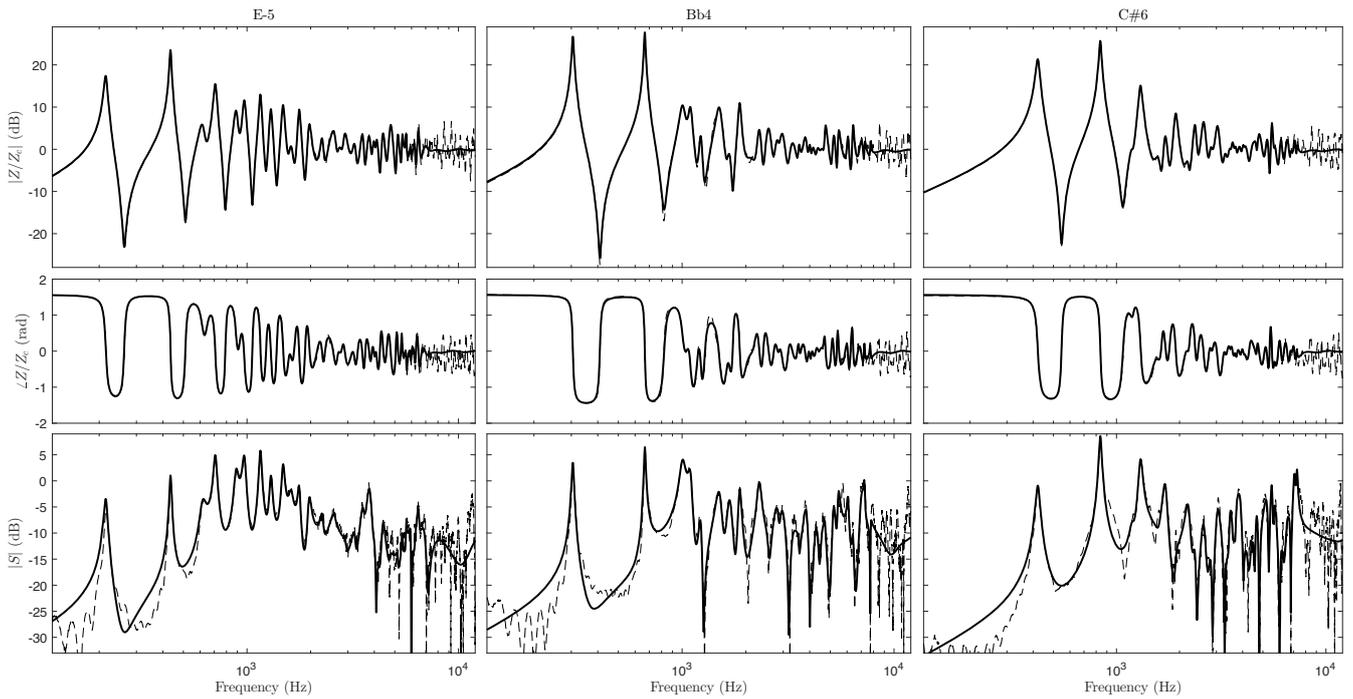
Figure 3: *Example impedance and radiaton models. All three fingerings were modeled with $M = 32$ parallel sections each. From top to bottom: impedance magnitude response, impedance phase response, and radiation magnitude response. In each plot, dashed lines and thick lines are used to depict the measurement and the model respectively.*

straightforward to compute the scalar pressure $P(z)$ at the input of the air column via

$$P(z) = Z|_f(z)U(z). \tag{15}$$

Finally, from the air column pressure $P(z)$ it is possible to obtain the (reflected) outgoing pressure wave $P^-(z)$ by means of

$$P^-(z) = P(z) - P^+(z). \tag{16}$$

Because the formulation of the model (5) presents a parallel structure that we want to maintain, inverting $Z|_f(z)$ as it appears in equation (14) is impractical. To overcome this problem in the realization of the reflectance, we reformulate the impedance in a similar manner as we did for the input admittance of string instruments [7] (inspired by [11]). First, we rewrite each resonator $H|_{f,m}(z)$ of equation (5) as

$$H|_{f,m}(z) = 1 + z^{-1}H_p|_{f,m}(z), \tag{17}$$

with

$$H_p|_{f,m}(z) = \frac{c_0|_{f,m} + c_1|_{f,m}z^{-1}}{1 + a_1|_{f,m}z^{-1} + a_2|_{f,m}z^{-2}}, \tag{18}$$

$c_0|_{f,m} = -1 - a_1|_{f,m}$, and $c_1|_{f,m} = -a_2|_{f,m}$. Note that denominator coefficients are related to pole radius and angle by $a_1|_{f,m} = -2|p|_{f,m}|\cos(\angle p|_{f,m})$ and $a_2|_{f,m} = |p|_{f,m}|^2$. We now can rewrite the impedance model as

$$Z|_f(z) = B_0|_f + z^{-1}B_1|_f + z^{-1}H_0|_f(z) + z^{-2}H_1|_f(z), \tag{19}$$

with

$$B_0|_f = \sum_{m=1}^{M|_f} b_0|_{f,m}, \quad B_1|_f = \sum_{m=1}^{M|_f} b_1|_{f,m}, \tag{20}$$

$$H_0|_f(z) = \sum_{m=1}^{M|_f} b_0|_{f,m}H_p|_{f,m}(z), \tag{21}$$

$$H_1|_f(z) = \sum_{m=1}^{M|_f} b_1|_{f,m}H_p|_{f,m}(z). \tag{22}$$

With this new formulation, we rewrite (14) and (15) as

$$U(z) = \frac{2Y_cP^+(z) - z^{-1}Y_cV|_f(z)U(z)}{1 + Y_cB_0|_f} \tag{23}$$

and

$$P(z) = B_0|_fU(z) + z^{-1}V|_f(z)U(z), \tag{24}$$

where

$$V|_f(z) = B_1|_f + H_0|_f(z) + z^{-1}H_1|_f(z). \tag{25}$$

It is important to notice that now the parallel structure appears in the numerator terms $H_0|_f(z)$ and $H_1|_f(z)$ as part of $V|_f(z)$, making possible its implementation. Moreover, $H_0|_f(z)$ and $H_1|_f(z)$ can be jointly implemented as a sole bank of parallel resonators. Finally, it is worth mentioning that the term $z^{-1}V|_f(z)U(z)$ appears in both equations (23) and (24) but does not need to be implemented twice–once it has been computed to obtain $U(z)$ via equation (23), it can be reused to compute $P(z)$ via equation (24).

5.2. External radiation realization

For the realization of the external radiation model, we take advantage of the fact that the flow $U(z)$ is available as an intermediate step in the computation of the reflected pressure vave $P^-(z)$. Using the decomposition described in (21) for each of the common resonators $H|_{f,m}(z)$, we rewrite the f-th radiation model $E|_f(z)$ in (12) as

$$E|_f(z) = D_0|_f + z^{-1}D_1|_f + z^{-1}L_0|_f(z) + z^{-2}L_1|_f(z), \quad (26)$$

with

$$D_0|_f = \sum_{m=1}^{M|_f} e_0|_{f,m}, \quad D_1|_f = \sum_{m=1}^{M|_f} e_1|_{f,m}, \quad (27)$$

$$L_0|_f(z) = \sum_{m=1}^{M|_f} e_0|_{f,m} H_p|_{f,m}(z), \quad (28)$$

$$L_1|_f(z) = \sum_{m=1}^{M|_f} e_1|_{f,m} H_p|_{f,m}(z). \quad (29)$$

With this, the radiated sound pressure signal $T(z)$ is computed as

$$T(z) = \left(D_0|_f + z^{-1}D_1|_f + z^{-1}L_0|_f(z) + z^{-2}L_1|_f(z)\right)U(z). \quad (30)$$

Please note that all four terms $H_0|_f(z)$, $H_1|_f(z)$, $L_0|_f(z)$, $L_1|_f(z)$ share inputs and parallel structure: each resonator $H_p|_{f,m}(z)$ is present in all four expressions (21), (22), (28), (29) and driven by the flow signal $U(z)$. Therfore, only one bank of $M|_f$ resonators needs to be implemented for the joint realization of the f-th fingering reflectance and external radiation models.

6. MODEL MIXING FOR FINGERING TRANSITIONS

So far, we have treated the impedance and radiation models of each f-th fingering as two parallel structures sharing a bank of resonators. Then we have derived a joint reflectance-radiation filter that simultaneously implements both models and can be interfaced to a reed model as a loaded waveguide termination. Such f-th termination filter replicates the behavior of the air column as observed during the f-th measurement. This means that for each fingering position we have a different termination filter, and in the context of sound synthesis this creates a fundamental problem: how to swap filters when a fingering transition happens? To avoid such an abrupt, non-physical operation we propose to reformulate our air column model as follows.

We define a sole impedance model $Z(z)$ that accounts for all F fingerings simultaneously, via a linear combination of all F single-fingering impedance models. This is expressed as

$$Z(z) = \sum_{f=1}^{F} w|_f Z|_f(z), \quad (31)$$

where $w|_f$ are mixing weights. Assuming that all F models $Z|_f(z)$ are positive-real, we guarantee that the multi-fingering input impedance model $Z(z)$ will be positive-real if all mixing weights are non-negative. With this, $Z(z)$ will lead to a passive termination irrespective of the weights applied in the linear combination. Thus, since fingering transitions are expected to happen at a sufficiently slow speed so that during each simulation step the whole system can be assumed to be quasi-static, a simple time-varying linear

mixing of any two impedance models can be used for a smooth, stable transition between fingerings.

For the external radiation model we apply the same idea, leading to a sole radiation model

$$E(z) = \sum_{f=1}^{F} w|_f E|_f(z), \quad (32)$$

where $w|_f$ match those used for impedance mixing. Now it is straightforward to rewrite the expressions for the joint reflectance-radiation realization. First, the impedance model is written as

$$Z(z) = B_0 + z^{-1}B_1 + z^{-1}H_0(z) + z^{-2}H_1(z), \quad (33)$$

where each of the terms is simply a linear combination of each of single-fingering terms in (20) through (22), leading to

$$B_0 = \sum_{f=1}^{F} w|_f B_0|_f, \quad B_1 = \sum_{f=1}^{F} w|_f B_1|_f, \quad (34)$$

$$H_0(z) = \sum_{f=1}^{F} w|_f H_0|_f(z), \quad (35)$$

$$H_1(z) = \sum_{f=1}^{F} w|_f H_1|_f(z). \quad (36)$$

With this, we also rewrite (23) and (24) as

$$U(z) = \frac{2Y_c P^+(z) - z^{-1}Y_c V(z)U(z)}{1 + Y_c B_0} \quad (37)$$

and

$$P(z) = B_0 U(z) + z^{-1}V(z)U(z), \quad (38)$$

where

$$V(z) = B_1 + H_0(z) + z^{-1}H_1(z). \quad (39)$$

An analogous transformation is applied to the radiation part of the model, leading to

$$E(z) = D_0 + z^{-1}D_1 + z^{-1}L_0(z) + z^{-2}L_1(z), \quad (40)$$

where

$$D_0 = \sum_{f=1}^{F} w|_f D_0|_f, \quad D_1 = \sum_{f=1}^{F} w|_f D_1|_f, \quad (41)$$

$$L_0(z) = \sum_{f=1}^{F} w|_f L_0|_f(z), \quad (42)$$

$$L_1(z) = \sum_{f=1}^{F} w|_f L_1|_f(z), \quad (43)$$

and the radiated sound pressure is again computed via

$$T(z) = \left(D_0 + z^{-1}D_1 + z^{-1}L_0(z) + z^{-2}L_1(z)\right)U(z). \quad (44)$$

In Figure 4 we display the input impedance magnitude, input impedance phase, and external radiation magnitude response of the model during a transition from E-5 to Bb4. It is worth noting that, although the complete model will in principle be constructed from all F resonators banks, its run-time operation logic can be implemented as follows: when no transition is happening, one bank of resonators is active; during a transition, two resonator banks are active.
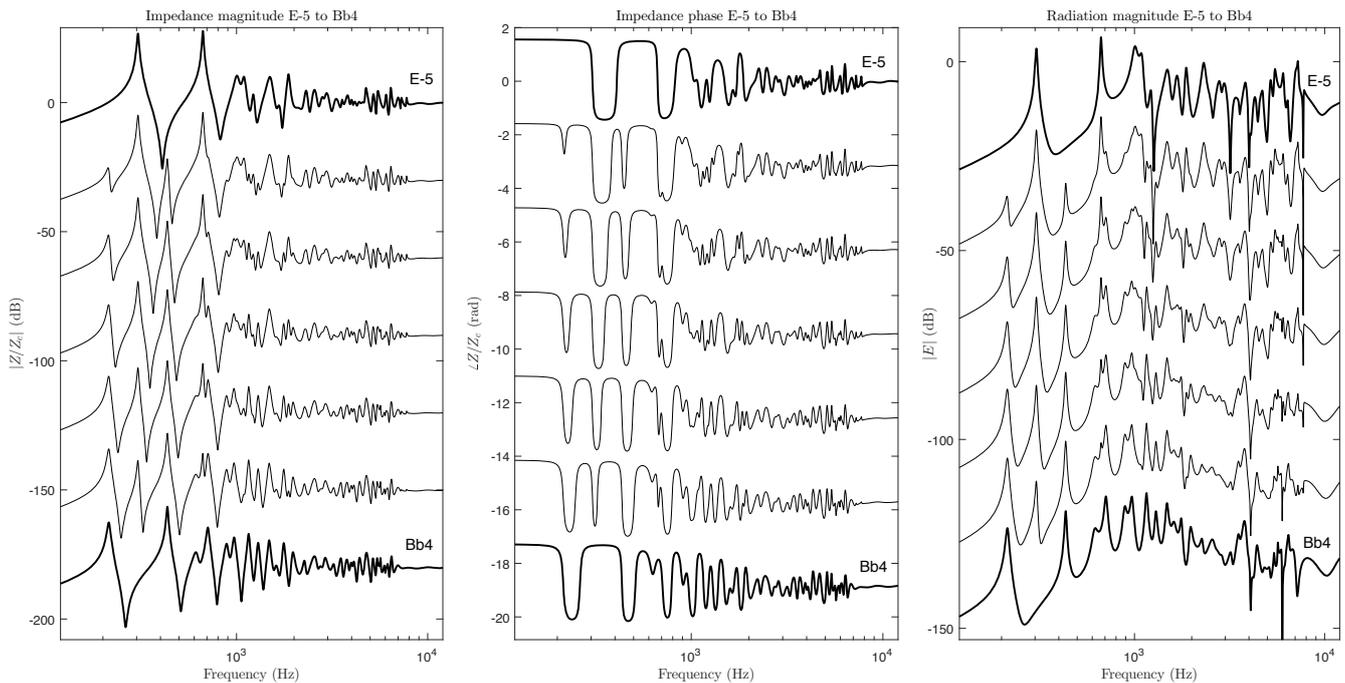
Figure 4: *Impedance and radiation model responses during a fingering transition, from E-5 to Bb4 positions. A linear mixing of 5 steps is performed from the corresponding impedance and radiation models, with $M = 32$ parallel sections each. Thick lines are used to depict the original E-5 (top) and Bb4 (bottom) models, and thin lines are used for the intermediate models. For clarity, impedance magnitude responses, impedance phase responses, and radiation magnitude responses were respectively offset by -30 dB, π radians, and -20 dB per step.*

7. DIGITAL WAVEGUIDE SOUND SYNTHESIS

We construct an efficient sound synthesis scheme by interfacing our joint reflectance-radiation model and a modified version of the digital waveguide reed scattering model used in [12] as follows. At each iteration, two main computations are interleaved: the reed scattering update and the air column reflectance update. During the reed scattering update, the differential pressure driving both the reed motion and the reed channel flow relation (see [12]) is first computed as the difference between the mouth pressure and the value of the scalar air column pressure obtained in the previous reflectance update (see Section 5.1). Then, the pressure wave obtained from the reed scattering is used to feed the next reflectance update. For an average of 32 resonators per fingering, a sampling frequency of 48 kHz, and fingering transitions sparsely happening for about 10% of the simulated time, this model runs at a speed above 30 times faster than real-time in one core of a laptop computer.

In Figure 5 we display the control signals (mouth pressure, fingering weights) and radiated sound of a synthesis example involving two fingering transitions: Bb4 to E-5 and E-5 to A-4, respectively happening at around 1.4 and 2.0 seconds. The first of these transitions involves nominal regimes in both fingerings, while for the second case the high mouth pressure drives the system into its higher octave regime after the transition. With respect to the transition happening at around 0.6 seconds, it does not involve any fingering change but is caused by the system falling from its higher-octave regime to its nominal regime. In Figure 6 we display the reed channel flow (see [12]), the air column input pressure, and the radiated sound during the Bb4 to E-5 transition of the example

in Figure 5. The synthetic radiated sound corresponding to this example can be heard online[1].

8. OUTLOOK

Albeit still exploratory and in need of a thorough calibration via automated playability analysis, our results open a promising route for efficient, yet realistic sound synthesis of wind instrument sound with potential applications both in rendering music and in analyzing the timbre and playability of real air column prototypes. Besides the application of this method to modeling other wind instrument air columns, a clear next stage of development involves the use of more sophisticated reed representations, and also the exploration of lip-driven excitation models. Perhaps through subjective tests, it is still necessary to investigate the effects of using more (or less) resonators per fingering, and also different fingering weight profiles. Perhaps through measurements, we could elucidate how well the cross-fading of models during fingering transitions simulates the actual case. Another of the extensions that we are considering involves coupling this model to a vocal tract model also realized as a reflectance that is interfaced to the valve model.

9. REFERENCES

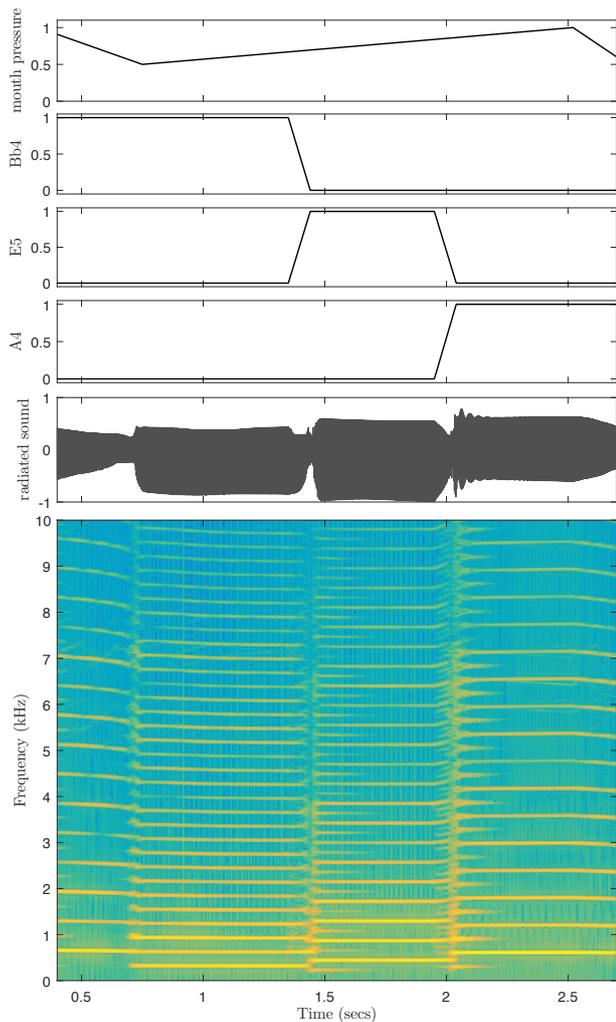[1] Julius O. Smith, *Physical Audio Signal Processing*, W3K Publishing, 2004, https://-

---

[1]http://ccrma.stanford.edu/~esteban/wind/dafx2018.wav

[6] E. Maestre, J. O. Smith, and G. P. Scavone, "Analysis-synthesis of saxophone input impedances via recursive parallel filters," in *Proc. of the International Symposium on Musical Acoustics*, 2017.

[7] E. Maestre, G. P. Scavone, and J. O. Smith, "Joint modeling of bridge admittance and body radiativity for efficient synthesis of string instrument sound by digital waveguides," *IEEE Transactions on Audio, Speech, and Language Processing*, vol. 25:5, pp. 1128–1139, 2017.

[8] A. Lefevbre and G. P. Scavone, "A comparison of saxophone impedances and their playing behavior," in *Proc. of the Forum Acusticum Conference*, 2011.

[9] J. Nocedal and S. J. Wright, *Numerical Optimization*, Springer, 2006.

[10] E. Maestre, G. P. Scavone, and J. O. Smith, "Design of recursive digital filters in parallel form by linearly constrained pole optimization," *IEEE Signal Processing Letters*, vol. 23:11, pp. 1547–1550, 2016.

[11] M. Karjalainen, "Efficient realization of wave digital components for physical modeling and sound synthesis," *IEEE Transactions on Audio, Speech, and Language Process.*, vol. 16:5, pp. 947–956, 2008.

[12] G. P. Scavone and J. O. Smith, "A stable acoustic impedance model of the clarinet using digital waveguides," in *Proc. of the International Conference on Digital Audio Effects*, 2006.

Figure 5: *Sound synthesis example, with $M = 32$ parallel sections per fingering. From top to bottom: mouth pressure (normalized units), weights w_f corresponding to Bb4, E-5, and A-4 fingerings, radiated sound pressure (normalized units), and a spectrogram of the radiated sound pressure.*

ccrma.stanford.edu/~jos/pasp.

[2] David P. Berners, *Acoustics and Signal Processing Techniques for Physical Modeling of Brass Instruments*, Ph.D. thesis, Stanford University, 1999, https://ccrma.stanford.edu/~dpberner/.

[3] G. Scavone, "Time-domain synthesis of conical bore instrument sounds," in *Proc. of the International Computer Music Conference*, 2002.

[4] F. Silva, C. Vergez, P. Guillemain, J. Kergomard, and V. Debut, "Moreesc: a framework for the simulation and analysis of sound production in reed and brass instruments," *Acta Acustica united with Acustica*, vol. 100(1), pp. 126–138, 2014.

[5] B. Gazengel, J. Gilbert, and N. Amir, "From the measured input impedance to the synthesis signal: where are the traps?," *Acta Acustica*, vol. 3, pp. 445–472, 1995.
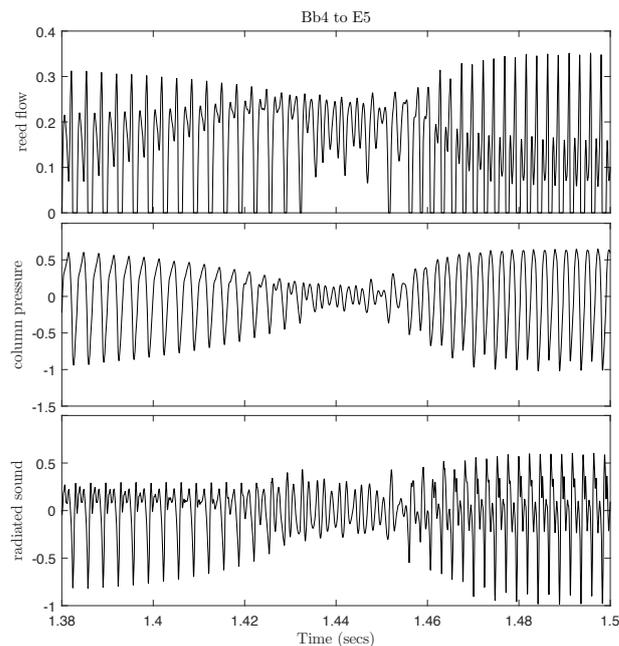
Figure 6: *Detail of the transition beween Bb4 to E-5. From top to bottom, in normalized units: reed flow, air column input pressure, radiated sound pressure.*